Anisotropic Magneto-Thermopower in M/Co/M ($M = \mathrm{Cu}, \mathrm{Pd}, \mathrm{Pt}$) Trilayer Systems

V. Popescu, P. Kratzer

published in

NIC Symposium 2016
K. Binder, M. Müller, M. Kremer, A. Schnurpfeil (Editors)

Forschungszentrum Jülich GmbH,
John von Neumann Institute for Computing (NIC),
Schriften des Forschungszentrums Jülich, NIC Series, Vol. 48,
ISBN 978-3-95806-109-5, pp. 217.
http://hdl.handle.net/2128/9842

Anisotropic Magneto-Thermopower in M/Co/M ($M = \mathrm{Cu}, \mathrm{Pd}, \mathrm{Pt}$) Trilayer Systems

Voicu Popescu and Peter Kratzer

Faculty of Physics and CENIDE, University Duisburg-Essen,
Lotharstr. 1, 47048 Duisburg, Germany
E-mail: {voicu.popescu, peter.kratzer}@uni-due.de

Ab initio investigations performed within the framework of the spin-polarised relativistic Korringa-Kohn-Rostoker Green's function method show that the longitudinal thermopower in the metallic M/Co/M systems (with M a non-magnetic transition metal) depends in a significant manner on the relative orientation (in-plane versus out-of-plane) of the sample magnetisation. As thermoelectric analogue of the conventional anisotropic magneto-resistance (AMR), the amplitude of this magneto-thermopower (MTP) signal is related to the asymmetry of the AMR around the Fermi energy. This asymmetry can be sizable, and thus the MTP accordingly large, even if the AMR itself is small. An enhancement of the MTP based on this understanding opens the possibility of implementing efficient spin read-out thermoelectric devices based on a single ferromagnetic layer. Our calculations reveal a rather non-intuitive behaviour of the MTP in the investigated systems, with the Pd/Co/Pd trilayer exhibiting an extremely small valued MTP, not necessarily expected from the monotonous increase of the spin-orbit coupling strength for the different heterostructure partners $M = \mathrm{Cu}, \mathrm{Pd}, \mathrm{Pt}$.

1 Introduction

Electron spin injection, manipulation and detection are the primary targets[1] of any application within the rich field of spintronics[2]. Exploiting the spin dependence of thermoelectric phenomena triggered, in addition, the fast development of a new branch, termed spin caloritronics[3,4]. Successful reports on thermally driven spin injection[5] and on detecting a magnetic response of the longitudinal thermopower in multilayered metallic nanowires[6] and tunnelling junctions[7] suggested the possibility of a practical magneto-thermoelectric device implementation.

While at the core of spintronics lies the electron spin degree of freedom, this, in turn, is coupled to the translational degree of freedom by virtue of the spin-orbit interaction. This ever present phenomenon is at the origin of a magnetisation orientation dependence of various ground state, excited state or transport properties. For the latter case, the most common example is the conventional anisotropic magneto-resistance (AMR)[8,9]: The resistivity (or, equivalently, the conductivity) of a ferromagnetic sample depends on the relative orientation between its magnetisation direction and that of the current. In the general terms of the electronic transmission probability $\mathcal{T}_{\vec{M}}(E)$ at energy E, this quantity will depend on the magnetisation $\vec{M}$ of the sample and the difference

$$\Delta\mathcal{T}(E) = \mathcal{T}_{\vec{M}_1}(E) - \mathcal{T}_{\vec{M}_2}(E) \tag{1}$$

between two different magnetic configurations $\vec{M}_1$ and $\vec{M}_2$ will be a direct measure of the AMR. In the case of a sizeable $\Delta\mathcal{T}$, it becomes obvious that one can use this effect as a magnetic read-out device. While in normal transition metal alloys and heterostructures this

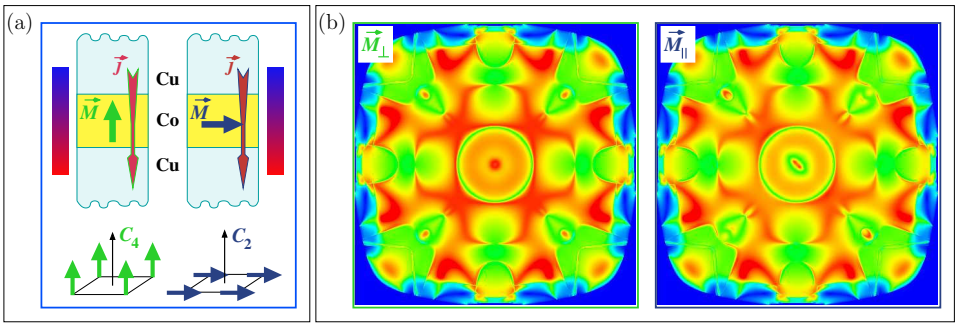

Figure 1. Illustration of spin-orbit coupling induced magnetic anisotropy manifestation in a thin Co slab embedded in Cu: (a) sketch of the geometry of the setup considered for the longitudinal anisotropic magneto-thermopower. The current density vector and the temperature gradient are oriented perpendicular to the interface, while the magnetisation is either perpendicular (green) or parallel (dark blue) to it. (b) Calculated electronic transmission probability $\mathcal{T}(\vec{k}_\parallel, E)$, Eq. 4, for the two different orientations of the magnetisation, $\vec{M}_\perp$ and $\vec{M}_\parallel$, in a 4 monolayer thick Co slab embedded in Cu. The transmission channels $\vec{k}_\parallel$ cover the full 2D Brillouin zone and the energy argument E is fixed. Note that the lowering of the symmetry illustrated in panel (a), from $\vec{M}_\perp$ configuration to $\vec{M}_\parallel$ is accordingly reflected in the two transmission profiles of panel (b).

effect is usually very small, such a setup has been successfully used to generate a typical low/high resistance spin-valve signal similar to that of the giant magneto-resistance (GMR) systems in tunnelling junctions[10]. These so-called Dirac devices have the major technological advantage of providing a spin resolution through a single ferromagnetic layer.

As an alternative, the read-out of such a logical element could also be accomplished by making use of the magneto-thermopower (MTP) effect that has been measured for various systems[11–14]. This effect, the thermoelectric equivalent of the AMR, can be described completely analogously: under a temperature gradient $\vec{\nabla}T$, the generated longitudinal thermopower $S(T)$ (Seebeck effect) takes on different values, depending on the angle between the sample magnetisation and $\vec{\nabla}T$:

$$\Delta S(T) = S_{\vec{M}_1}(T) - S_{\vec{M}_2}(T) \neq 0 \ , \tag{2}$$

where $\vec{M}_1$ and $\vec{M}_2$ have the same meaning as above.

An illustration of such a setup is provided in Fig. 1(a). The longitudinal MTP signal is generated by a a single magnetic layer (here, without restricting the generality, taken to be Co) sandwiched between two non-magnetic leads (here Cu). The magnetic anisotropy occurring in this system is caused by the symmetry break-off at the interface, as illustrated, for the case of a quadratic two-dimensional (2D) lattice in Fig. 1(a). Upon this junction one can apply either an electric field or a thermal gradient *perpendicular* to the Co/Cu interface and detect an AMR or an MTP response by flipping the magnetisation direction from perpendicular ($\vec{M}_\perp$) to parallel ($\vec{M}_\parallel$) to the interface. We have primarily focused on the correlation between the MTP and the conventional AMR, establishing a practical way to maximise the former.

Our first results for Cu/Co/Cu(001) trilayers[15], obtained by *ab initio* spin-polarised relativistic calculations that account directly, in a parameter free way, for the simultaneous manifestation of spin polarisation and spin-orbit coupling[16], have shown that both AMR

and MTP have a common origin: the spin-orbit coupling induced anisotropy in the electronic transmission probability. The calculated MTP was found to have a large value over a wide range of temperatures and Co thickness values. We could establish, in addition, that the MTP is maximised by an enhanced asymmetry in the AMR energy dependence. Indeed, rather than mapping the Fermi-surface alone, the thermoelectric phenomena depend on transmission channels extending over a finite interval around the Fermi energy.

These investigations are hereby extended to the M/Co/M (111)-oriented trilayers ($M = \mathrm{Cu}, \mathrm{Pd}, \mathrm{Pt}$). Our results reveal that, while Pt/Co/Pt and Cu/Co/Cu systems exhibit a sizeable MTP, the Pd-based trilayers are characterised by a very small anisotropic thermoelectric response, in spite of having a rather large AMR, comparable to that of Pt/Co/Pt. The outcome of our study is two-fold: The MTP-AMR relationship is generally applicable, however, a large MTP signal is indeed not conditioned by the size but rather by a stark energy dependence of the AMR.

2 Theoretical Aspects and Computational Details

2.1 Geometry Setup and Self-Consistent Potentials

Our investigations on the trilayer systems involve two steps. First, we perform self-consistent electronic structure calculations for both magnetic configurations $\vec{M}_\perp$ and $\vec{M}_\parallel$ using a spin-polarised relativistic implementation[16] of the screened Korringa-Kohn-Rostoker Green's function method (KKR-GF)[17–19], combined with the decimation technique[20] for 2D-periodic systems.

A prototypical trilayer system consists of two half-infinite M leads with an interaction region inserted in-between, all sharing the same in-plane 2D periodic lattice. The interaction region contains the n-monolayer (ML) thick Co slab and up to 10 MLs of the heterostructure partner M on both sides of the Co slab. We have considered one of the metals adopting the in-plane lattice constant of its partner, thus being subject to epitaxial strain and manifesting a tetragonal distortion. With the in-plane lattice fixed, the vertical inter-layer separation was determined using continuum elasticity. In our calculations we use spherical potentials in the atomic sphere approximation (ASA) determined within the local spin-density approximation[21]. An angular momentum cut-off of $l_{max} = 3$ was taken for the Green's function expansion and $2\,l_{max} = 6$ for the charge density.

2.2 Transport Properties

In a second step, the self-consistent potentials are used as input for a calculation scheme that relies on a relativistic implementation[22] of the Landauer-Büttiker formula within the KKR-GF method[23]. This provides the electron transmission probability $\mathcal{T}_{\vec{M}}(E)$ at energy E for the magnetic configuration $\vec{M}$:

$$\mathcal{T}_{\vec{M}}(E) = \frac{1}{A_{2D-BZ}} \int_{2D-BZ} d^2\vec{k}_\parallel \mathcal{T}_{\vec{M}}(\vec{k}_\parallel, E) \ , \tag{3}$$

obtained as an integral over the 2D Brillouin zone (2D-BZ) of the single-channel, ballistic transmission probability $\mathcal{T}_{\vec{M}}(\vec{k}_\parallel, E)$ for a 2D vector $\vec{k}_\parallel$[23]. This latter quantity can be determined from the z-component of the current operator $\underline{J}$ and the Green's function matrices

$\underline{G}$[22,23] (omitting the configuration index $\vec{M}$):

$$\mathcal{T}(\vec{k}_{\parallel}, E) = \sum_{n \in L} \sum_{n' \in R} \mathrm{Tr} \left[\underline{J}_n^{\mathrm{T}}(E) \underline{G}_{nn'}(\vec{k}_{\parallel}, E) \underline{J}_{n'}(E) \underline{G}_{nn'}^{\dagger}(\vec{k}_{\parallel}, E) \right] \tag{4}$$

for atoms n (n') belonging to the left (right) lead, where the underscored symbols designate matrices in the relativistic representation (j, m_j).

The energy dependent transmission given in Eq. 3 is used to determine the transport coefficients[24]:

$$L_{\vec{M}}^{(\alpha)}(T) = \int dE \left[\left(-\frac{\partial f_0}{\partial E} \right) \mathcal{T}_{\vec{M}}(E) \ (E - \mu)^{\alpha} \right] \ , \tag{5}$$

with $f_0(E, T, \mu)$ the Fermi-Dirac distribution function at energy E, temperature T and chemical potential μ. Knowledge of these quantities allows one to calculate the Seebeck coefficient $S_{\vec{M}}(T)$ as[24]:

$$S_{\vec{M}}(T) = -\frac{1}{eT} \frac{L_{\vec{M}}^{(1)}}{L_{\vec{M}}^{(0)}} \ . \tag{6}$$

The formalism sketched here only considers the electronic temperature, neglecting the electron-phonon or electron-magnon scattering. As these effects are less important at low temperatures, we have restricted our investigations to a temperature range below 350 K and focused on phenomena solely related to the changes in the electronic structure induced by modifying the magnetic configuration of the system. We finally note that the dependence of the self-consistent potentials and the transport properties on the magnetisation direction is implicitly taken into account by solving the Dirac equation in the local frame of reference at each atomic site and then applying unitary rotations to transform into the global frame of reference with the quantisation axis parallel to the z-axis[16].

2.3 Relationship between the MTP and AMR

The way in which a transmission probability profile $\mathcal{T}_{\vec{M}}(E)$ influences the sign and size of the Seebeck coefficient at finite temperatures can be understood on the basis of Eq. 6. In this equation, a temperature increase effectively extends the integration range, by increasing the non-zero width of $\mathcal{T}_{\vec{M}}(E)(\partial f_0/\partial E)$. Because of the $(E - E_{\mathrm{F}})$ term, the numerator can be seen as a centre of mass of $\mathcal{T}_{\vec{M}}(E)(\partial f_0/\partial E)$[25]. Consequently, both sign and value of $S_{\vec{M}}(T)$ will be sensitive even to small changes in the numerator's integrand below or above E_{F}. This behaviour illustrates the simple path towards maximising the Seebeck coefficient of a sample, by achieving a strongly asymmetric $\mathcal{T}_{\vec{M}}(E)$ around E_{F}.

The AMR in typical transition metal systems, alloys or heterostructures, is rather small, not exceeding few percent. We show in Fig. 1(b) the full transmission profiles $\mathcal{T}_{\vec{M}}(\vec{k}_{\parallel}, E)$ calculated for $\vec{M} \equiv \vec{M}_{\perp}$ and $\vec{M} \equiv \vec{M}_{\parallel}$ configurations over the whole 2D-BZ in a Cu/Co_4/Cu(001) trilayer. The energy argument corresponds to $E = E_{\mathrm{F}} - 0.14$ eV, chosen in such a way that $\Delta\mathcal{T}(E)$ attains a local maximum. We make two important observations: (i) the $\mathcal{T}_{\vec{M}}(\vec{k}_{\parallel}, E)$ contours clearly reflect the lowering of the symmetry when switching from $\vec{M}_{\perp}$ to $\vec{M}_{\parallel}$ configuration (from four-fold to two-fold rotation axis); and

(ii) it is rather difficult to note quantitative differences between the two quantities. In fact, explicit evaluation of Eq. 3 led to a $\Delta\mathcal{T}(E)$ difference in the range of $4\ \%$.

The latter is an important observation in establishing a direct connection between the magnitude of the MTP signal and the asymmetry of the AMR around the Fermi energy. On its basis, one can make the reasonable approximation that the zero-order transport coefficient, Eq. 5, has a negligible dependence on $\vec{M}$, such that $L^{(0)}_{\vec{M}_\perp}(T) \simeq L^{(0)}_{\vec{M}_\parallel}(T)$. It follows, from the definition of the Seebeck coefficient, Eq. 6, that the MTP introduced in Eq. 2 can be expressed as

$$\Delta S(T) \propto \int dE(\partial_E f_0)(E - E_F)\,\Delta\mathcal{T}(E)\ , \tag{7}$$

with $\Delta\mathcal{T}(E)$ given by Eq. 1. From this equation it can be seen that, since $(E - E_F)$ is anti-symmetric about E_F, a $\Delta\mathcal{T}(E)$ of odd parity about E_F is needed to maximise the MTP. We emphasise here on the analogy with the condition for $S(T)$, which is maximised by an asymmetry of $\mathcal{T}(E)$.

2.4 Use of Computer Resources

As outlined above, the central quantity to be calculated for the electronic transport investigations is the $\vec{k}_\parallel$- and E-resolved transmission probability $\mathcal{T}_{\vec{M}}(\vec{k}_\parallel, E)$ given by Eq. 4. Closer inspection of this equation reveals that, amongst its two ingredients – the current density operator $\underline{J}_n$ and the structural Green's function matrix $\underline{G}_{nn'}(\vec{k}_\parallel, E)$ – only the latter depends on the transmission channel $\vec{k}_\parallel$. Since the evaluation of Eq. 4 essentially implies a trace of a matrix product, one can easily separate and optimise the integration loops required in this formula. This leads to an efficient parallelisation over the energy and $\vec{k}_\parallel$ variables.

In spite of this convenient form and the additional advantages brought about by the screened KKR method (essentially an order-N method), the calculation of the transmission probability and of the Seebeck coefficient remains a quite tedious and computationally demanding task: (i) The integration range in Eq. 5 is, in principle, infinite; in practice, however, it can be restricted to a domain in which the derivative of the Fermi-Dirac is greater than a user-defined "zero", a quantity which needs to be tested basically for every system; (ii) The $k_\parallel$-resolved transmission $\mathcal{T}_{\vec{M}}(\vec{k}_\parallel, E)$, Eq. 4, may be a fast-varying, non-monotonous function of $\vec{k}_\parallel$, as seen in Fig. 1(b). Convergence tests have shown that the number of $\vec{k}_\parallel$-points needed to ensure the convergence of $\mathcal{T}_{\vec{M}}(E)$ at any energy in the proximity of μ has to be in the order of 10^6.

3 MTP versus AMR in M/Co/M ($M = \mathrm{Cu, Pd, Pt}$)

Having established the link between the MTP and the AMR via Eq. 7, we have focused on the following issues: (i) is the MTP-maximisation recipe provided by Eq. 7 generally valid? (ii) does the inclusion of a material, such as Pt and Pd, with a higher spin-orbit coupling (SOC) and hence a higher AMR necessarily lead to an increase of the MTP?

We illustrate our results for the case of an M/Co_6/M (111)-oriented heterostructure (M = Cu, Pd and Pt) with a fixed thickness of the ferromagnetic Co layer. Fig. 2(a)

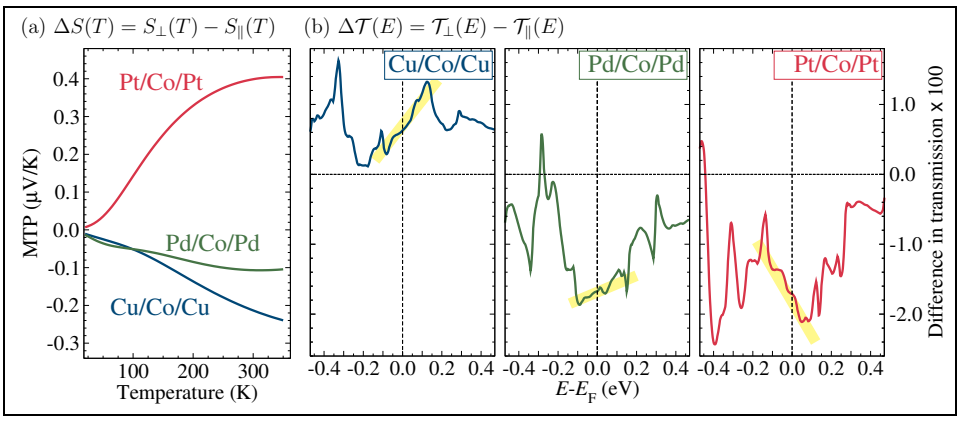

Figure 2. (a) The magneto-thermopower in the M/Co$_6$/M (111)-oriented trilayers ($M = \mathrm{Cu}, \mathrm{Pd}, \mathrm{Pt}$) and (b) the difference in the electronic transmission probability for the magnetisation oriented perpendicular and parallel to the M/Co interface in a current-perpendicular-to-the-plane (CPP) setup for the same systems, from left to right. The different slopes around the Fermi energy (taken as reference) are highlighted as guide for the eyes.

displays the calculated MTP, $\Delta S = S_\perp - S_\parallel$, in the three systems [Eq. 2 and lhs of Eq. 7], while panel (b) of the figure shows, from left to right for each M, the calculated energy-dependent AMR, $\Delta\mathcal{T}(E) = \mathcal{T}_\perp(E) - \mathcal{T}_\parallel(E)$ [Eq. 1 and the integrand of the rhs of Eq. 7]. In addition, the different slopes of $\Delta\mathcal{T}(E)$around the Fermi energy (taken as reference) are highlighted as guide for the eyes in Fig. 2(b).

As seen in Fig. 2(a), Pt/Co/Pt and Cu/Co/Cu systems are characterised by rather large MTP values, in the order of few tenths of μV/K, negative for Cu and positive for Pt. These values of $\Delta S(T)$ need to be compared with the calculated Seebeck coefficients for the respective systems (not shown here), which lie in the range of -5 μV/K (in Cu/Co/Cu) and ± 1 μV/K (in Pd/Co/Pd and Pt/Co/Pt). This effectively corresponds to an MTP response as high as $\simeq$ 35 % for the Pt/Co/Pt system. In contrast, the highest calculated AMR, found for the same heterostructure, does not exceed 2 % [note the multiplicative factor 100 in Fig. 2(b)], at typical values for $\mathcal{T}(E)$ in the order of unity. In other words, using the MTP effect as a basis for a spin read-out Dirac device might be more efficient than through a conventional AMR element.

The Pd-based heterostructure stands out through its extremely small anisotropic MTP effect, as compared to the other two non-magnetic metals. This behaviour might appear counter-intuitive at a first glance, since the SOC increases as going downwards in the periodic table, 3d→4d→5d. One notes, on the other hand, that the AMR *does* follow the expected trend, with $\Delta\mathcal{T}(E)$ increasing along the series Cu-Pd-Pt.

This apparent disagreement with what an educated guess might suggest can be relatively easily understood on the basis of the established link between the MTP and the AMR expressed by Eq. 7. It becomes clear that both sign *and* magnitude of the calculated MTP correlate with the *slope* of $\Delta\mathcal{T}(E)$ around the Fermi energy [highlighted in Fig. 2(b)], which is nothing else but the expected result from Eq. 7: since the integrand contains the product $(\partial_E f_0)(E - E_F)\,\Delta\mathcal{T}(E)$ with $\partial_E f_0$ of even and $(E - E_F)$ of odd symmetry with respect to E_F, the integral is zero for $\Delta\mathcal{T}(E)$ even, being maximised by

an as asymmetric as possible AMR. This analysis answers the two issues raised above: (i) numerical results confirm that the MTP-AMR connection expressed by Eq. 7 is quite general; and (ii) a large AMR is not *alone* a sufficient ingredient to ensure a maximum MTP signal. Indeed, as evidenced by the comparison of the $\Delta\mathcal{T}(E)$ profiles for Pd/Co/Pd and Pt/Co/Pt in Fig. 2(b), the two systems differ less in the magnitude of the AMR as in its *energy dependence* around the Fermi energy E_F. In conclusion, we have shown, for a series of heterostructures containing a ferromagnetic layer in a trilayer configuration with non-magnetic leads, a general recipe to enhance the MTP. This may in principle enable the implementation of efficient spin read-out thermoelectric devices based on a single ferromagnetic layer, with significant technological advantages over the, often very complex, multilayer spin valves.

Acknowledgements

This work was supported by the German Research Foundation within the Priority Program 1538 "Spin Caloric Transport (SpinCaT)". The authors gratefully acknowledge the computing time granted by the John von Neumann Institute for Computing (NIC) and provided on the supercomputer JUROPA at Jülich Supercomputing Centre (JSC).

References

1. I. Žutić, J. Fabian, and S. Das Sarma, *Spintronics: Fundamentals and applications*, Rev. Mod. Phys., **76**, 323–410, 2004.
2. E. Y. Tsymbal and I. Žutić, (Eds.), *Handbook of Spin Transport and Magnetism*, Chapman and Hall/CRC Press, Boca Raton, FL, USA, 2011.
3. G. E. W. Bauer, E. Saitoh, and B. J. van Wees, *Spin caloritronics*, Nature Materials, **11**, 391–399, 2012.
4. B. Scharf, A. Matos-Abiague, I. Žutić, and J. Fabian, *Theory of thermal spin-charge coupling in electronic systems*, Phys. Rev. B, **85**, 085208, Feb 2012.
5. A. Slachter, F. L. Bakker, J. P. Adam, and B. J. van Wees, *Thermally driven spin injection from a ferromagnet into a non-magnetic metal*, Nature Physics, **6**, 879–882, 2010.
6. L. Gravier, S. Serrano-Guisan, F. Reuse, and J.-P. Ansermet, *Thermodynamic description of heat and spin transport in magnetic nanostructures*, Phys. Rev. B, **73**, 024419, 2006.
7. M. Walter, J. Walowski, V. Zbarsky, M. Münzenberg, M. Schäfers, D. Ebke, G. Reiss, A. Thomas, P. Peretzki, M. Seibt, J. S. Moodera, M. Czerner, M. Bachmann, and C Heiliger, *Seebeck effect in magnetic tunnel junctions*, Nature Materials, **10**, 742–746, 2011.
8. J. Smit, *Magnetoresistance of ferromagnetic metals and alloys at low temperatures*, Physica, **17**, 612 – 627, 1951.
9. I. A. Campbell, A. Fert, and O. Jaoul, *The spontaneous resistivity anisotropy in Ni-based alloys*, Journal of Physics C: Solid State Physics, **3**, S95, 1970.

10. C. Gould, C. Rüster, T. Jungwirth, E. Girgis, G. M. Schott, R. Giraud, K. Brunner, G. Schmidt, and L. W. Molenkamp, *Tunneling Anisotropic Magnetoresistance: A Spin-Valve-Like Tunnel Magnetoresistance Using a Single Magnetic Layer*, Phys. Rev. Lett., **93**, 117203, 2004.
11. Y. Pu, E. Johnston-Halperin, D. D. Awschalom, and J. Shi, *Anisotropic Thermopower and Planar Nernst Effect in* $\mathrm{Ga}_{1-x}\mathrm{Mn}_x\mathrm{As}$ *Ferromagnetic Semiconductors*, Phys. Rev. Lett., **97**, 036601, 2006.
12. P. Wiśniewski, *Giant anisotropic magnetoresistance and magnetothermopower in cubic 3:4 uranium pnictides*, Applied Physics Letters, **90**, 192106, 2007.
13. A. D. Avery, M. R. Pufall, and B. L. Zink, *Observation of the Planar Nernst Effect in Permalloy and Nickel Thin Films with In-Plane Thermal Gradients*, Phys. Rev. Lett., **109**, 196602, 2012.
14. A. D. Avery, M. R. Pufall, and B. L. Zink, *Determining the planar Nernst effect from magnetic-field-dependent thermopower and resistance in nickel and permalloy thin films*, Phys. Rev. B, **86**, 184408, 2012.
15. V. Popescu and P. Kratzer, *Large Seebeck magnetic anisotropy in thin Co films embedded in Cu determined by ab initio investigations*, Phys. Rev. B, **88**, 104425, 2013.
16. H. Ebert, D. Ködderitzsch, and J. Minár, *Calculating condensed matter properties using the KKR-Green's function method - recent developments and applications*, Rep. Prog. Phys., **74**, 096501, 2011.
17. L. Szunyogh, B. Újfalussy, P. Weinberger, and J. Kollár, *Self-consistent localized KKR scheme for surfaces and interfaces*, Phys. Rev. B, **49**, 2721–2729, 1994.
18. R. Zeller, P. H. Dederichs, B. Újfalussy, L. Szunyogh, and P. Weinberger, *Theory and convergence properties of the screened Korringa-Kohn-Rostoker method*, Phys. Rev. B, **52**, 8807, 1995.
19. K. Wildberger, R. Zeller, and P. H. Dederichs, *Screened KKR-Green's-function method for layered systems*, Phys. Rev. B, **55**, 10074–10080, 1997.
20. I. Turek, V. Drchal, J. Kudrnovský, M. Šob, and P. Weinberger, *Electronic Structure of Disordered Alloys, Surfaces and Interfaces*, Kluwer Academic Publishers, Boston, 1997.
21. S. H. Vosko, L. Wilk, and M. Nusair, *Accurate spin-dependent electron liquid correlation energies for local spin density calculations: a critical analysis*, Canadian Journal of Physics, **58**, 1200, 1980.
22. V. Popescu, H. Ebert, N. Papanikolaou, R. Zeller, and P. H. Dederichs, *Influence of spin-orbit coupling on the transport properties of magnetic tunnel junctions*, Phys. Rev. B, **72**, 184427, 2005.
23. Ph. Mavropoulos, N. Papanikolaou, and P. H. Dederichs, *Korringa-Kohn-Rostoker Green-function formalism for ballistic transport*, Phys. Rev. B, **69**, no. 15, 125104, 2004.
24. U. Sivan and Y. Imry, *Multichannel Landauer formula for thermoelectric transport with application to thermopower near the mobility edge*, Phys. Rev. B, **33**, 551–558, 1986.
25. M. Czerner, M. Bachmann, and C. Heiliger, *Spin caloritronics in magnetic tunnel junctions: Ab initio studies*, Phys. Rev. B, **83**, 132405, 2011.